Light Manipulation and Applications
https://doi.org/10.70401/lma.2026.0016

Supplementary information

Polarization-insensitive RGBN color router based on metasurface

Yunlai Fu, Xiujuan Zou, Jiawang Chen, Ruihan He, Quan Yuan, Haoxiang Yu, Shuming Wang

S1.Spectral Response of Conventional Color Filters

The spectral sensitivity range of silicon-based complementary metal-oxide-semiconductor (CMOS) photodetectors covers from ultraviolet to near-infrared wavelengths. Conventional Bayer arrays employ low-pass filters to block near-infrared light to prevent image fading. Without these filters, infrared data extraction is not feasible. The spectral response of the novel "red, green and blue + near-infrared" (RGBN) color filter array is depicted in **Figure S1**. By introducing a dedicated NIR channel, the sensor's light reception can be effectively enhanced, enabling the capture of near-infrared images.

S2.Principles of Material Selection

The complex refractive index $m(\lambda)=n(\lambda)+i\kappa(\lambda)$ controls the metasurface response through two coupling mechanisms. First, the real part $n(\lambda)$ determines the optical path and effective phase delay of each meta-atom, which is approximately $\varphi \approx \frac{2\pi}{\lambda} n_{eff}(\lambda) h$. There needs to be sufficient refractive index contrast between Si_3N_4 and the surrounding medium to provide strong phase and amplitude modulation within a limited thickness; if $n(\lambda)$ is too low, the phase coverage and scattering intensity are insufficient, so less energy is routed to the target pixel and more light leaks to adjacent pixels. Conversely, too high or strongly dispersive $n(\lambda)$ may enhance local/Mie resonances or waveguide resonances. This can increase peak efficiency at selected wavelengths, but also tends to make the spectral more sensitive to manufacturing errors and angle of incidence. Therefore, $n(\lambda)$ mainly determines the routing peak position, bandwidth and inter-channel crosstalk through the effective phase and the dispersion of the resonant mode. Secondly, the extinction coefficient κ, or the equivalent absorption coefficient $\alpha = 4\pi\kappa / \lambda$,directly reduces the available optical power through intensity attenuation $\exp(-\alpha h)$. Any non-zero or wavelength-dependent κ will reduce the overall energy utilization efficiency.

To ensure a high energy utilization efficiency in the color router, it is essential to select transparent materials with high refractive indices that exhibit minimal absorption in the range of 400-1,100 nm for the metasurface. Si_3N_4 and TiO_2 are commonly used materials for metasurface spanning from visible light to near-infrared, given their mature and stable fabrication processes. However, for the CR to be directly integrated with CMOS image sensors, fabrication must be carried out on photodiodes with SiO_2 layers. Therefore, the chosen material's fabrication process should not damage the substrate. In TiO_2 metasurface fabrication processes, using SiO_2 as a mask can lead to acid processes damaging the chip's film layers directly. Alternatively, employing metal Cr as a mask results in inadequate etching rate ratios between the etched material and the mask, posing challenges to ensure the protection of TiO_2 when reaching the target depth. In contrast, Si_3N_4 processes do not exhibit these drawbacks and ensure that the entire process operates at temperatures below 200 degrees, thereby safeguarding the CMOS photosensitive units. Hence, we opted for Si_3N_4 as the material for the design and fabrication of the RGBN-MBCR. The refractive index values (n and k) of the materials used are illustrated in **Figure S2**.

For real chip integration, we have proposed the following feasible solutions to some of the foreseeable problems based on the existing metasurface processing technology and CMOS technology: First, in terms of the uniformity of the film layer, existing PECVD and other solutions can already deposit uniform materials, and they can be further polished to ensure flatness. In terms of alignment accuracy, in order to ensure accurate alignment between metasurface and the pixel layer below, aligned mark needs to be prepared on the CIS. The alignment of edge pixels can be used to ensure the consistency between metasurface and pixel periods. Regarding temperature control, during the preparation of metasurface, all processes should be controlled below the melting point of silicon-based transistors and other metal materials (such as inter-pixel Al grids) to avoid structural deformation caused by long-term heating.

S3.Hyperparameters of Optimization and Computing Resource

In this paper, an optimization framework founded upon the principle of inverse design is established, wherein ANSYS Lumerical FDTD software is employed for electromagnetic modeling and simulation, while MATLAB's Genetic Algorithm Toolbox is utilized to optimize the structural parameters. In the specific design of the QR code-like structure, we concurrently consider computational resource constraints and manufacturing capability limitations. By partitioning the entire periodic unit into $n \times n$ grid, the design degrees of freedom amount to 2^n, such that a smaller edge length of the meta-atom increases the number of degrees of freedom and provides greater design flexibility; however, this also leads to a substantial increase in the convergence time of the optimization algorithm. At the same time, existing lithography techniques cannot support excessively fine line widths. Therefore, we set n = 16, meaning each meta-atom has an edge length of 125 nm. The fabrication of the silicon nitride (Si_3N_4) metasurface is a nuanced process, constrained by the risk of structural collapse due to high aspect ratios. To avert such calamities, the parameter h is meticulously optimized within a range spanning 500 nm to 1,000 nm. Moreover, the envisaged utilization of the RGBN-MBCR primarily involves its integration onto CIS chips. This integration necessitates the deposition of a SiO_2 layer onto the chip's light-sensitive unit before metasurface-fabrication. To maintain structural integrity and avert fracturing, this layer's thickness is limited to a few micrometers, prompting the optimization range for parameter f to be delineated from 1 μm to 5 μm.

We initially generate a random initial population in MATLAB, inputting the matrix parameters into Lumerical FDTD to establish a single-period metasurface model. Periodic boundary conditions are applied in the ±x and ±y directions, with Perfect Match Layer (PML) conditions set along the z-axis. The incident light source is configured as a plane wave spanning wavelengths from 400 to 1,100 nm, and four monitors with light source limits are positioned on the router plane, representing target pixels of different colors. Solving Maxwell's equations within FDTD yielded the transmittance for each monitor, and the fitness function is calculated by using predefined weighting factors v. This fitness function's value is then fed back into MATLAB to update the population and obtain new matrix parameters. This process is repeated, iteratively optimizing the matrix parameters to reduce the fitness function value until convergence to a global minimum. The algorithm's maximum iteration limit is 150 generations, but if the improvement of fitness function is less than 0.001 for 20 consecutive generations or more, the algorithm terminates early and outputs the current results.

Differential design for specific incident conditions is an important step towards engineering in the future. Following the principles and working methods of the microlens array in CIS, we can add incident angle restrictions during the optimization process, redesign the larger chief ray angle, or use the lens shift method to ensure the angular robustness of the RGBN-MBCR array.

The convergence process curve optimized by genetic algorithms is illustrated in **Figure S3**. Since the genetic algorithm toolbox used can only solve for minima, a negative sign is added before the fitness function in the main text to meet this requirement. Throughout the optimization process, each generation's matrix is stored and compared with the previous fitness function. If the fitness remains unchanged for 30 consecutive generations, the algorithm terminates early and outputs the current optimal solution. In order to avoid falling into the local optimal solution, we added dynamic optimization of parameters to the reversely designed genetic algorithm and used a higher initial mutation rate. If the calculation time is acceptable, increase the population size appropriately. Additionally, running multiple times is a simple and effective avoidance measure. The finalized optimized structure is illustrated in **Figure S4**.

The hyperparameters used in the algorithm are as follows: population size:100, ConstraintTolerance:0.001, max generation:150. And the server and software configuration is as follows:

(a) CPU: AMD EPYC 7763 64-Core Processor@2.45GHz.
(b) RAM:128GB. Mesh size:50nm.
(c) Simulation time: about 40 seconds per simulation and over 60 hours for whole optimization.
(d) Boundary conditions: X & Y directions: Periodic; Z direction: PML.
(e) Monitor settings: use light source limits: true; Use wavelength spacing: true.

S4.Numerical Simulation of RGBN-MBCR

To showcase the polarization-insensitive characteristics of the metasurface we designed, we simulated the electromagnetic responses of light with different polarization angles and wavelengths passing through the RGBN-MBCR. **Figure 2**c,d depict the light field distributions on the routing plane for incident light at wavelengths of 450, 540, 630, and 900 nm with x and y polarizations, with **Figure S5** showing the distributions for other polarization angles. Furthermore, spectral curves at each pixel area under different incident conditions are calculated and illustrated in **Figure 2**e,f and **Figure S6.** It is evident that under all polarizations, incident light can be effectively separated and collected by the corresponding pixel areas. **Figure S7** demonstrates the simulated total energy utilization efficiency.

For the simulation of angular response, since the arrangement of RGBN is not symmetrical, we fixed the polarization angle to be consistent with the y-axis, and used the xz plane perpendicular to it as the plane of change of the incident angle. For the visible light band, each color pixel can still maintain a relatively obvious response at 10°, and its peak value is always above the 25% efficiency benchmark of the color filter, as shown in **Figure S8**. In this case, color routing functionality can still be implemented between RGB pixels. As the incident angle increases, the spectral response of each pixel will gradually broaden, especially the energy in the infrared band will be focused to the B pixel, and the R band energy will be focused to the G pixel. This is because the longer the wavelength, the more obvious the focus shift effect, which is the main factor restricting the performance of RGBN-MBCR.

S5.Sample Fabrication Process

A SiO_2 substrate is prepared using a cleaning process by ultrasonic. Then the Si_3N_4 film with 800-nm-thick is deposited over the cleaned substrate by plasma-enhanced chemical vapour deposition (PECVD, RSP 800). Electron beam photoresist and conductive adhesive (AR-P6200.04 and AR-PC5090.02) are then spin-coated. The optimized metasurface pattern is defined in the photoresist by electron beam lithography (EBL, Elionix, ELS-F125-G8). After the development of the resist, a layer of chromium(Cr) with the pattern array is evaporated onto the sample by electron beam evaporation(EBE). After performing lift-off, a Cr hard mask is left on the Si_3N_4 layer for subsequent etching. The sample is etched using an inductively coupled plasma and reactive ion etching etcher (ICP-RIE, Haasrode-E200) with a mixture of CF_4, SF_6 and CHF_3. Eventually, the rest Cr hard mask is removed using a corrosion solution called ammonium cerium nitrate. The flowchart of fabrication is shown in **Figure S9**. The entire process is conducted at temperatures below 200℃, at which point the circuits and photosensitive elements on the surface of standard CIS chips remain unaffected by physical or chemical damage. This provides crucial support for the subsequent integration of the meta-structure onto the chip. In the subsequent integration process, it is necessary to first deposit a layer of SiO_2 on the chip surface based on the optimized working distance f and the thickness d of the protective layer, and then perform the same metasurface preparation process as above.

S6.Characterization of RGBN-MBCR

To measure the light intensity distribution at different wavelengths on the routing plane, we utilized a broad-spectrum light source to illuminate the sample and customized a microscopic system for imaging the routing plane.

As shown in **Figure S10**a, the light emitted by the broad-spectrum white light source passes through the collimating lens and the imaging lens and then illuminates the RGBN-MBCR. Incident light can be made monochromatic by inserting different color filters, and the NA of the imaging lens can be adjusted. Objective lens, tube lens and monochrome camera together form an imaging system. By adjusting the distance between RGBN-MBCR and the imaging system, the routing plane can be clearly imaged in the screen. To characterize the polarization response, we inserted a linear polarizer as shown in **Figure S10**b. When simulating the image acquisition process based on RGBN-MBCR, we placed a 24-ColorChecker in front of the imaging lens and used a light source for uniform illumination. Adjust the position of the object so that it can be clearly imaged on the camera, as shown in **Figure S10**c. To compare the performance of MBCR and filters, we removed the RGBN-MBCR and inserted different filters. **Figure** 5f was taken with the optical setups shown in **Figure S10**d. The spectral distribution of the light source is depicted in **Figure S11**, which simulates the solar spectrum encompassing visible and infrared light. The sensitivity of the monochrome camera is shown in **Figure S12**.

By adjusting the displacement stage to position the sample's router plane at the working distance of the objective lens (20x magnification), the image is magnified and projected onto the monochrome camera. The spectral efficiency is defined as the ratio of the energy collected at a specific wavelength on each pixel to the total energy of that wavelength incident on the entire period, expressed as, $T_i = \frac{\int_{\sigma_i} I_i \mathrm{d}\sigma_i}{\sum_i \int_{\sigma_i} I_i \mathrm{d}\sigma_i}$, where $i = B, G, R, N$.

Normalization is necessary due to the non-uniform spectral distribution of the light source used in the experiment, leading to varying energy levels at different wavelengths, and the non-uniform response of the camera's photosensitive units to different wavelengths. By adding different narrow-band filters (width ≈ 10 nm) behind the light source, approximate monochromatic intensity distribution maps can be obtained (**Figure**

S12), and the spectral efficiency curves for each pixel, as shown in the main text **Figure 3d**, are calculated. The results are generally consistent with numerical simulations, with the primary errors stemming from lower energy levels of certain wavelength light sources or poor camera sensitivity.

To quantitatively evaluate the crosstalk level of the RGBN-MBCR, we define a crosstalk matrix $\boldsymbol{C}=\begin{bmatrix} C_{BB} & C_{GB} & C_{RB} & C_{NB} \\ C_{BG} & C_{GG} & C_{RG} & C_{NG} \\ C_{BR} & C_{GR} & C_{RR} & C_{NR} \\ C_{BN} & C_{GN} & C_{RN} & C_{NN} \end{bmatrix}$ to describe the energy coupling ratio between different wavelengths. $\boldsymbol{C}_{ij}$ represents the proportion of light intensity measured at the pixel of the j-color (target channel) when the incident light is of the i-color. A representative matrix estimated from **Figure 3d** is

$$\boldsymbol{C}=\begin{bmatrix} 0.374 & 0.198 & 0.204 & 0.224 \\ 0.158 & 0.368 & 0.247 & 0.227 \\ 0.136 & 0.278 & 0.471 & 0.115 \\ 0.229 & 0.189 & 0.223 & 0.359 \end{bmatrix}$$

The max crosstalk is 27.8%.

Figure S14 shows he relationship between light field distribution and NA changes. Color routing performance is maintained until NA=0.17. As NA increases, the focus point becomes blurred and significantly forms crosstalk with adjacent pixels at NA=0.26. The non-uniformity of light intensity distribution mainly comes from the processing error of the sample, and is also related to the tilt error of the measurement optical path and imperfect aberration correction.

The overall light collection efficiency of the sample was analyzed using a spectrometer, and the measured curves are illustrated in **Figure S15**. Across the entire 400-1,100 nm wavelength range, the average light collection efficiency reached 92.81%.

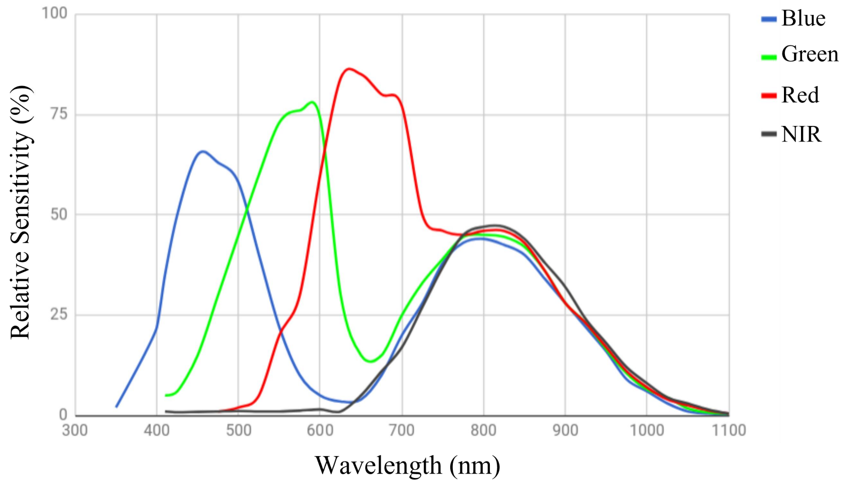

Figure S1. Sensitivity graph for single sensor camera with RGB-NIR filters. RGB: green and blue; NIR: near-infrared.

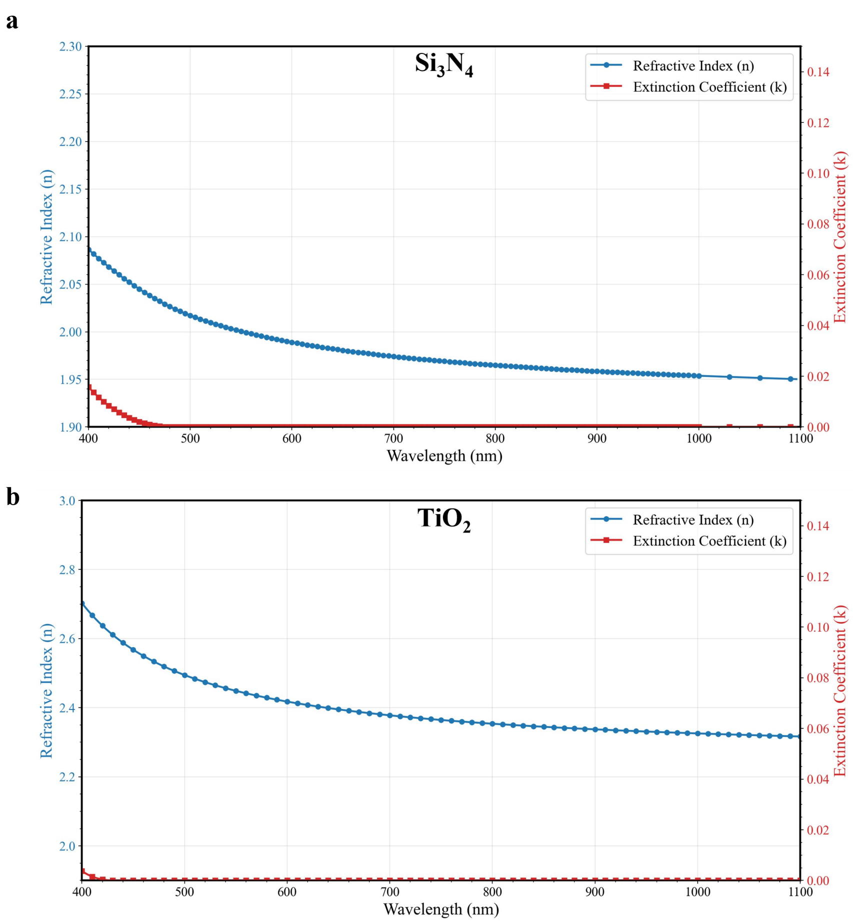

Figure S2. The refractive index in the light regime. (a) Si_3N_4; (b) TiO_2.

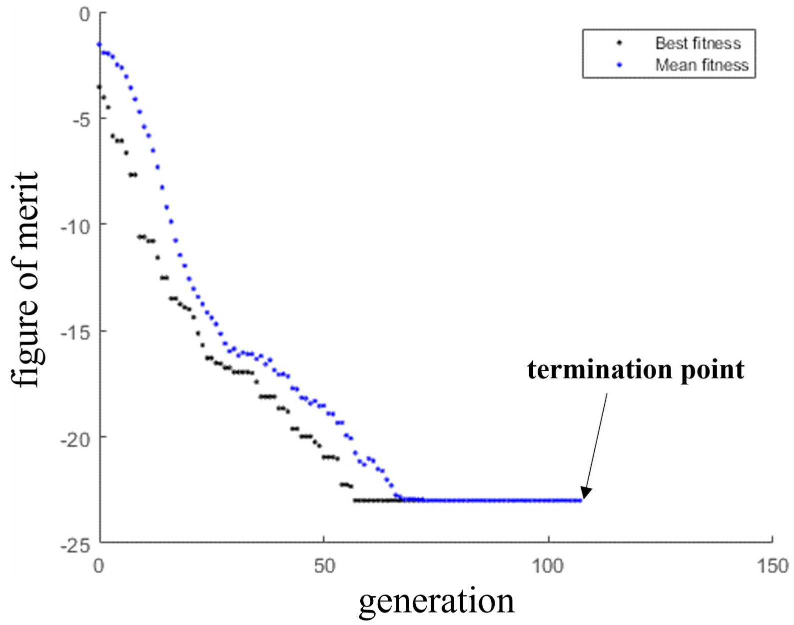

Figure S3. Convergence curve of the inverse design algorithm.

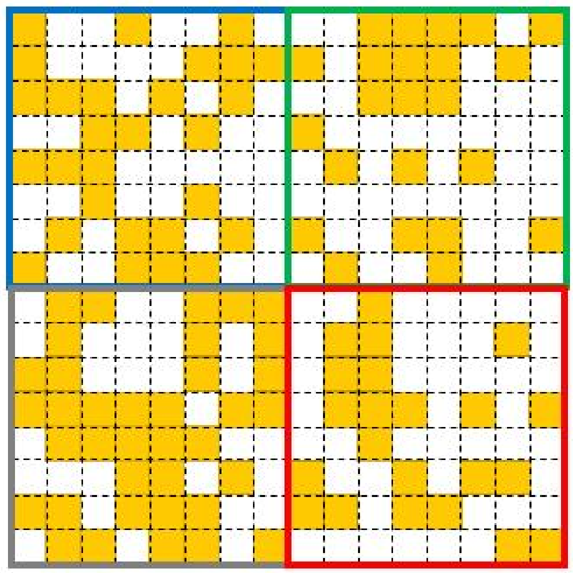

Figure S4. Binary distribution map of the optimized metasurface in the main text. The yellow squares represent Si3N4 and the whites represent air.

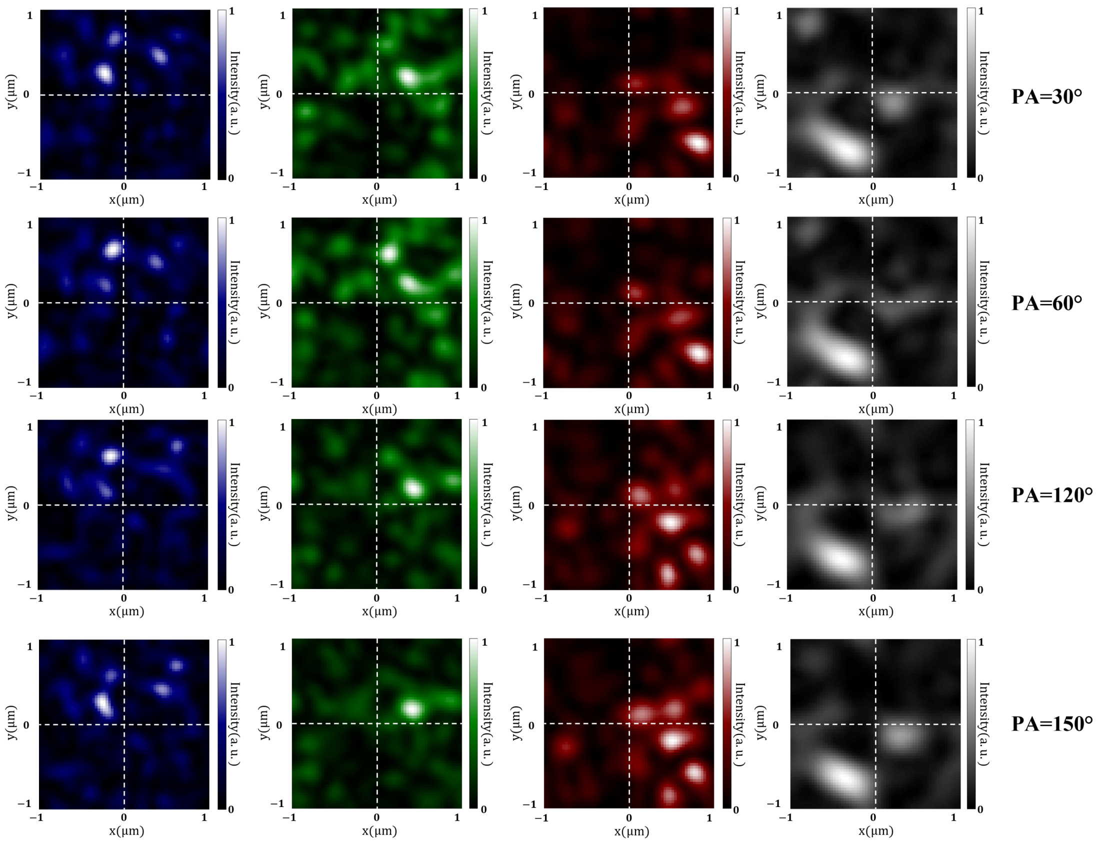

Figure S5. Intensity distribution across a single period under different PAs. PAs: polarization angles.

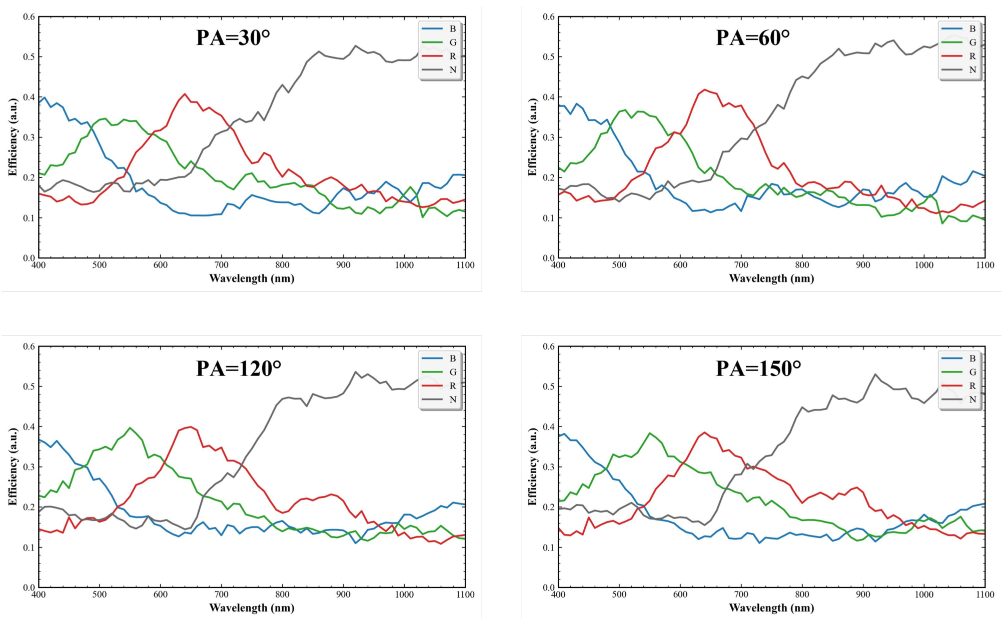

Figure S6. The simulated optical spectrum curves under different PAs. PAs: polarization angles.

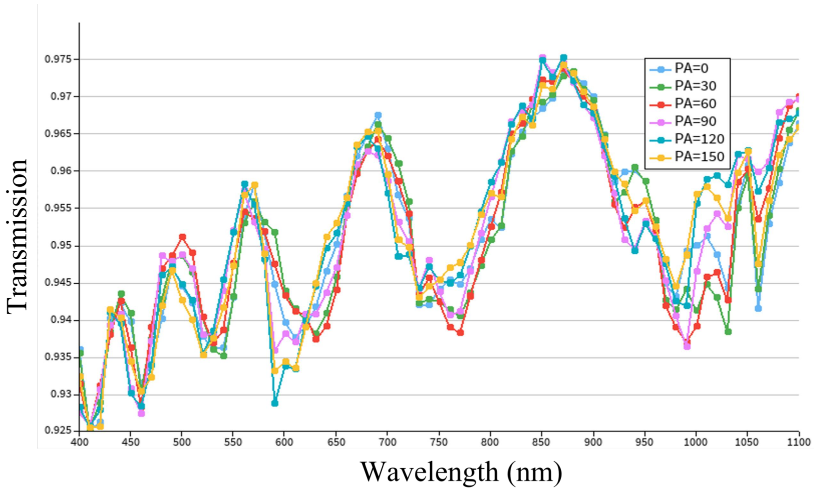

Figure S7. The simulated energy utilization efficiency under different PAs. PAs: polarization angles.

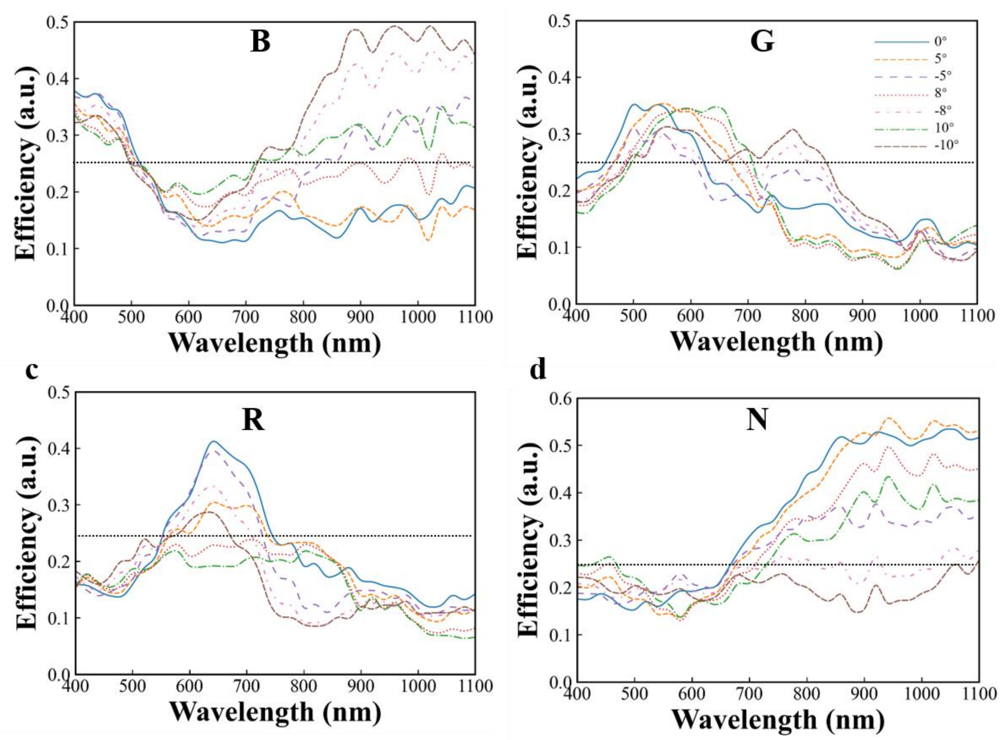

Figure S8. The simulated optical spectrum curves under different incident angles.

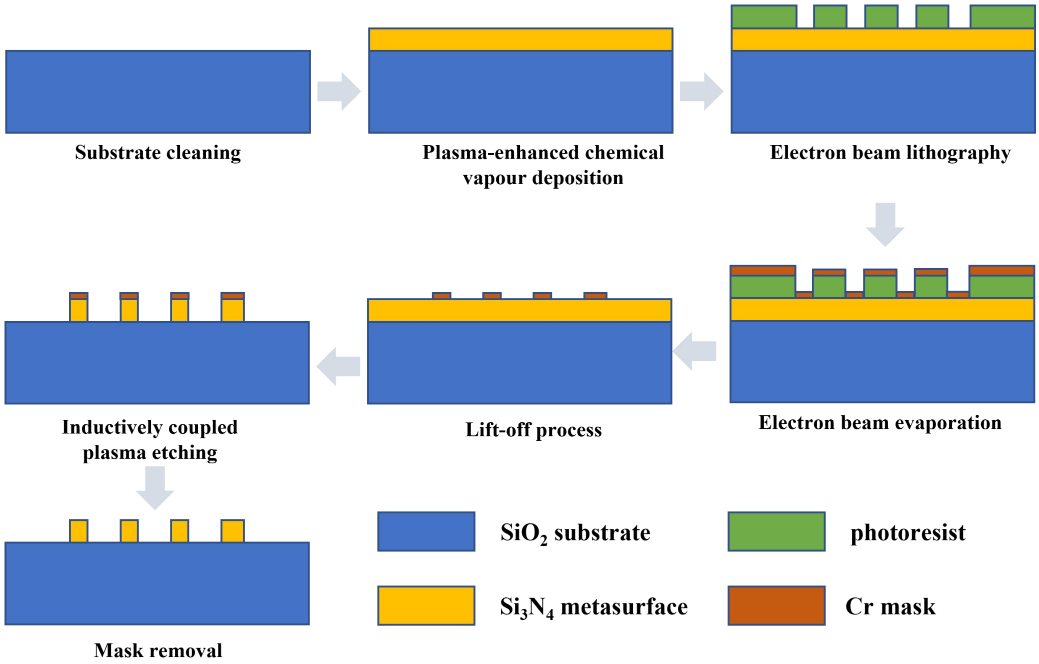

Figure S9. Flowchart of the preparation of the RGBN-MBCR sample. RGBN: red, green and blue + near-infrared; MBCR: metasurface-based color router.

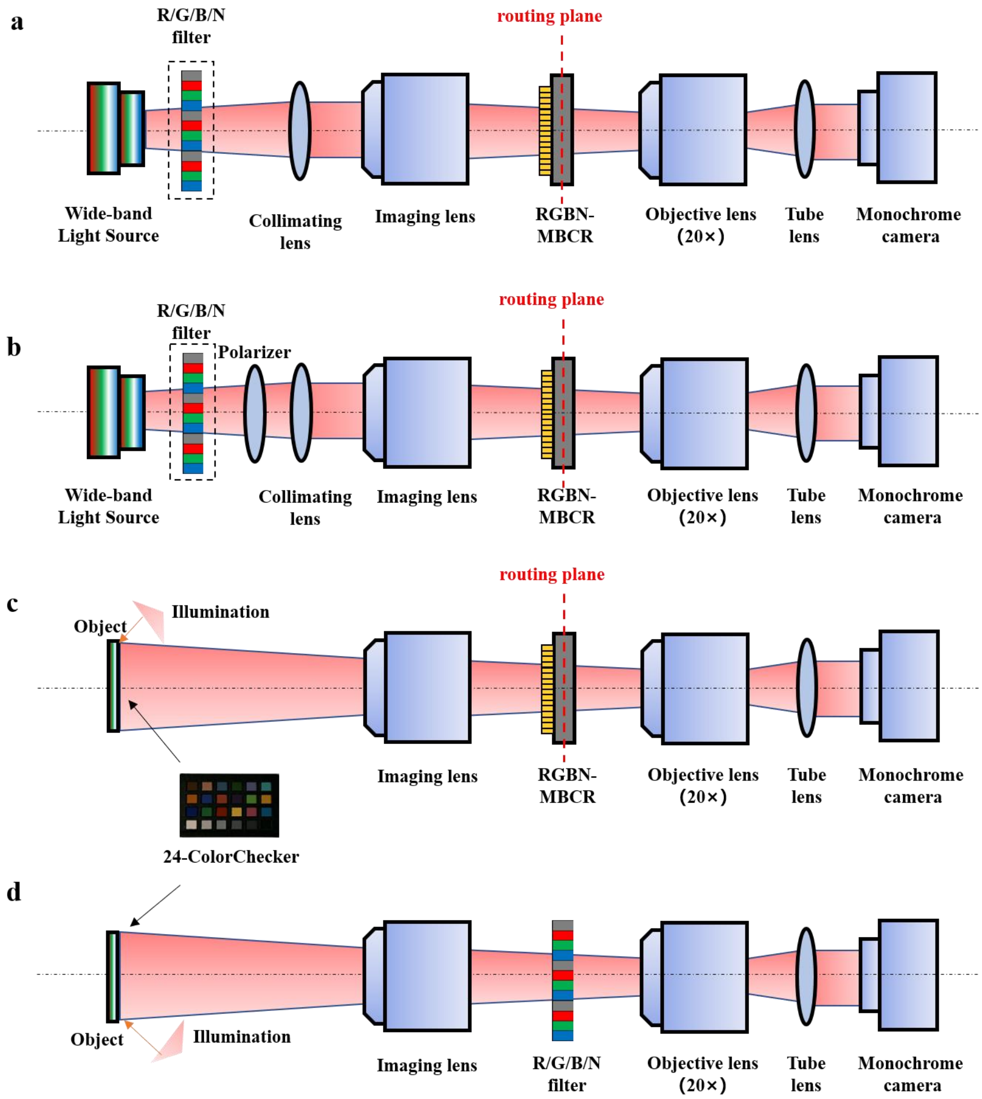

Figure S10. Experimental setups for measurements. (a) Experimental setup for characterizing the routing plane and light routing effect of RGBN-MBCR; (b) Experimental setup for characterizing the polarization sensitivity of RGBN-MBCR; (c) Experimental setup for the image acquisition process of an RGBN-MBCR-based sensor; (d) Experimental setup for the image acquisition process of traditional RGB-NIR sensor. RGBN: red, green and blue + near-infrared; MBCR: metasurface-based color router; NIR: near-infrared.

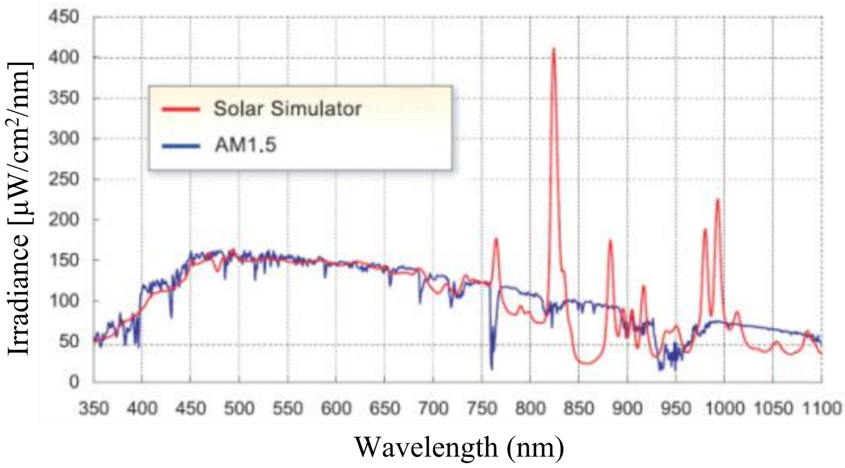

Figure S11. Spectral information of light source.

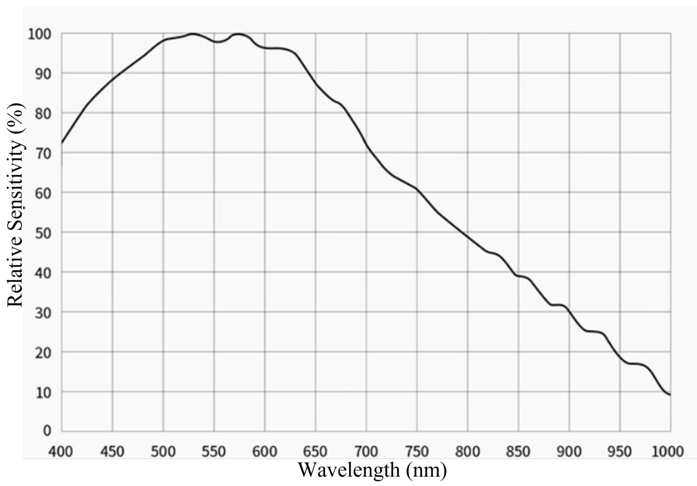

Figure S12. Spectral response curve of the camera used in the experiment.

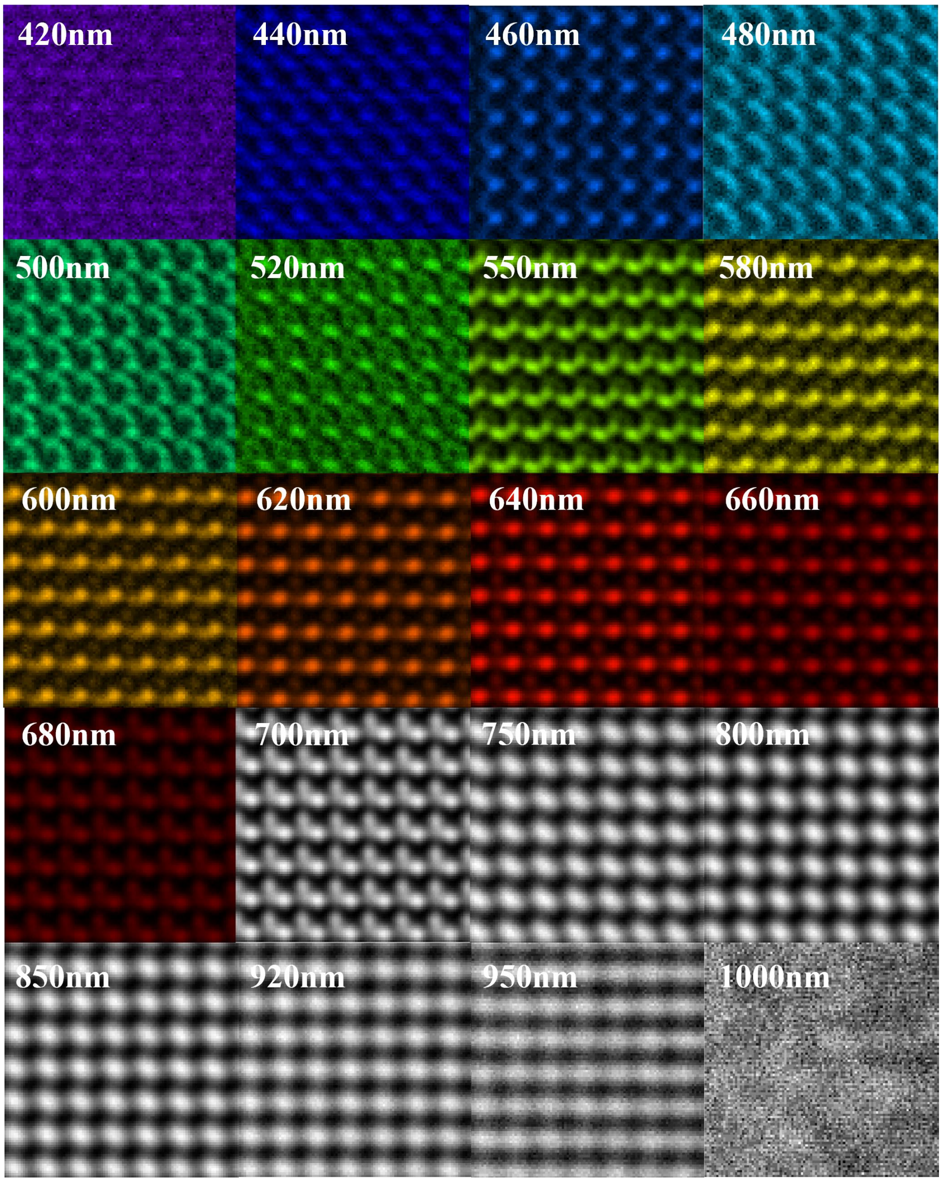

Figure S13. Measured light intensity distribution on the imaging plane under different wavelengths of incident light on a linear scale with the RGBN-MBCR. The wavelength of the incident light is labeled above each picture. RGBN: red, green and blue + near-infrared; MBCR: metasurface-based color router.

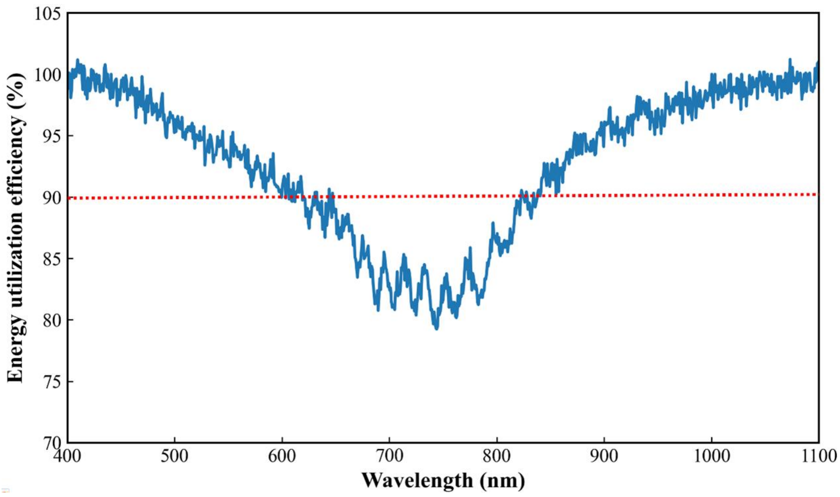

Figure S14. The measured energy utilization efficiency of RGBN-MBCR. The fluctuations in the curve are caused by interference effects resulting from variations in substrate thickness. RGBN: red, green and blue + near-infrared; MBCR: metasurface-based color router; NIR: near-infrared.

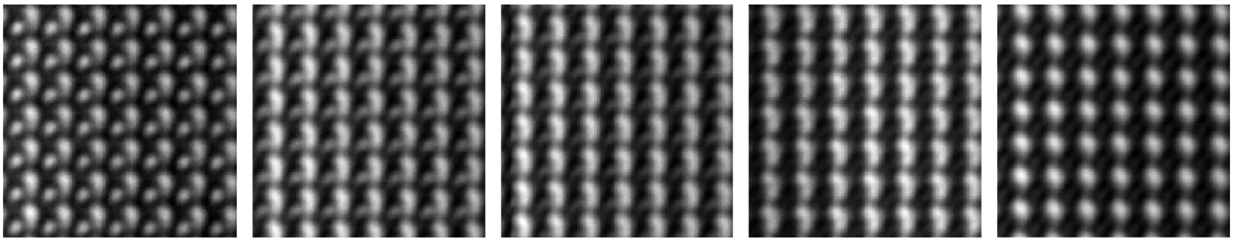

Figure S15. Influence of NA on routing performance. Images taken at different NA of 0.02, 0.14, 0.17, 0.21, 0.26. NA: numerical aperture.

Figure S16. The fused color image without CCM and WB. CCM: color correction matrice; WB: white balance.

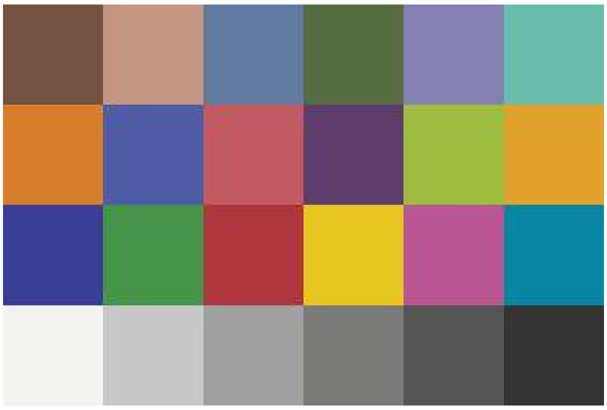

Figure S17. The standard colors of 24-ColorChecker.

Table S1. Correlation coefficients among the spectral curves of four pixels.

Pixel	Pearson product-moment correlation coefficient	Cosine similarity	Euclidean distance
B	0.968	0.9989	0.7735
G	0.988	0.9991	0.7654
R	0.981	0.9978	0.6969
N	0.986	0.9986	0.7420